厚生労働科学研究費補助金（医療機器開発推進研究事業）
分担研究報告書

ウィルスベクターを用いたアミロスフェロイドの機能解析に関する研究

研究分担者　村松慎一　自治医科大学・内科学講座神経内科学部門　特命教授

研究要旨
アミロスフェロイド(ASPD)の病態生理学的意義を明らかにし，アルツハイマー病の早期診断と治療法を開発することを目標として研究を行った．発達過程の影響を受けない新規のモデル動物を作製するためアデノ随伴ウイルス（AAV）を応用した．AAVのカプシド蛋白およびゲノム配列を改変し，広範な脳領域の神経細胞特異的にアミロイド前駆体蛋白質遺伝子を発現可能な血管内投与型AAVベクターを開発した．Sweden型変異を持つアミロイド前駆体蛋白質を発現するAAVベクターを脳内に投与したサルでは注入部位付近の扁桃体にASPD陽性の老人斑を認めた．

A. 研究目的

アルツハイマー病は，近年の高齢化人口の増加に伴い重要な社会問題となっている認知症（痴呆症）の主要な原因である．アルツハイマー病では，脳内にAβアミロイド蛋白の蓄積が認められ，Aβが神経細胞死を引き起こすと考えられている．Aβの神経毒性の機序を解明することは，アルツハイマー病の発症予防および治療法の開発のために重要である．

本研究は，Aβが球状の構造アミロスフェロイド(ASPD)をとることにより毒性を発揮するという星らの仮説をモデル動物で検証し新たな治療法を開発することを目的としている．

B. 研究方法

血管内投与後に脳内へ移行しやすいAAVベクターを見出すため各種の型のカプシド蛋白を持ち，蛍光蛋白質GFPを発現するpseudotype AAVベクターを作製した．一部の型では，カプシド蛋白のアミノ酸配列を置換し，発現カセットの塩基配列も改変したベクターを作製した．CAGプロモーターあるいは神経細胞特異的Synapsine Iプロモーターの下流にGFPのcDNAを繋ぎ，SV40 poly(A)配列とともに 3型AAVのinverted terminal repeats (ITR)配列の間に挿入した．

アミロイド前駆体蛋白(APP)蛋白を発現するAAVベクターを作製した．APPは野生型に加え，家族性アルツハイマー病のSweden型変異 ($Lys^{670}\rightarrow Asn^{670}$, $Met^{671}\rightarrow Leu^{671}$)およびE693Δ型についてもベクターを作製した．

作製した血管内投与型GFP発現AAVベクターを成体C57BL6マウスの血管内に投与し，4週間後に脳組織を回収し免疫組織化学を行った．

2008年9月にSweden型変異APPを発現するAAV8ベクター(AAV8-SynI-APPsw)を定位脳手術で投与したカニクイサルの脳組織を18か月後に還流固定しASPD抗体による免疫組織化学を行った．

C. 研究結果

野生型カプシドを持つAAV8, AAV9ベクターでは，脳内の少数の神経細胞およびグリア細胞にGFPの発現が認められた．

カプシド及びゲノム構造を改変し神経細胞特異的プロモーターを搭載した新規開発の血管内投与型AAVベクターでは，脳の広範な領域で多数の神経細胞にGFPの発現が認められた．

APP遺伝子(野生型，Sweden型，E693Δ型)を搭載した血管内投与型ベクターでは，*in vitro*でAPPの発現を確認した．

AAV8-SynI-APPswを投与したサルでは，注入部位付近の扁桃体にASPD陽性の老人斑を認めた．

（倫理面での配慮）

動物個体での実験手法は，法律第105 号「動物の愛護及び管理に関する法律」，総理府「実験動物の飼養及び保管に関する基準」，文部省通知「大学等における動物実験について」を遵守し，自治医大の動物実験委員会の承認を得て行った．

D. 考察

ASPDの病態解明と治療法の開発には，脳内にASPDを生じる適切なモデル動物が必要となる．ASPD自体を定位脳手術で注入する場合は，注入針の刺入に伴う急性の炎症とそれによるASPDの除去反応が生じる可能性が考えられる．そのため，AAVベクターにより持続的にAPPを発現させることにした．定位脳手術によるサル脳内へのAAVベクターの投与では，注入部位付近でASPD抗体陽

性の老人斑が認められ，ベクター未投与の対側では見られないことから，APP持続発現によりASPDが形成されたと考えられる．

血管内投与型AAVベクターによりAPP遺伝子を神経細胞で発現させる方法を開発した．このAAVベクターでは，脳内の広範な領域の神経細胞に効率よくAPP遺伝子を導入し長期発現させることが可能となる．血液脳関門を通過する詳細な機序は不明であるが，炎症反応や組織破壊は認めていない．今後，各APP遺伝子を搭載したベクターをマウスに投与し病態解析と治療法の開発を継続する．

E. 結論

脳内の広範な領域で ASPD を生じる新規モデル動物作製のため血管内投与型 AAV ベクターを開発した．

F. 健康危険情報

特になし

G.研究発表

1.論文発表

E. Krzyżosiak A, Szyszka-Niagolov M, Wietrzych M, Gobaille S, Muramatsu S, Krężel W. Retinoid X receptor gamma control of motivated behaviours involves dopaminergic signalling in mice. Neuron, 66(6):908-920, 2010.

F. Muramatsu S, Fujimoto K, Kato S, Mizukami H, Asari S, Ikeguchi K, Kawakami T, Urabe M, Kume A, Sato T, Watanabe E, Ozawa K, Nakano I. A phase I study of aromatic L-amino acid decarboxylase gene therapy for Parkinson's disease. Mol Ther, 18(9):1731-1735, 2010.

G. Muramatsu S, Asari S, Fujimoto K, Ozawa K, Nakano I: Gene therapy for Parkinson's disease. Strategies for the local production of dopamine. Gene Therapy & Regulation 5(1):57-65, 2010.

H. Muramatsu S: The current status of gene therapy for Parkinson's disease, Ann Neurosci, 17(2):92-95, 2010.

2. 学会発表

1. 村松慎一, 浅利さやか, 中村優子, 川上忠孝, 池口邦彦, 藤本健一, 中野今治：AADC 遺伝子導入による L -dopa反応性の変化. 第51回日本神経学会総会, 東京, 2010 年 5 月 20 日. (プログラム p69)

2. 浅利さやか, 藤本健一, 中野今治, 村松慎一, 齊藤順一, 佐藤俊彦, 宮内昭広：FMT-PET によるパーキンソン病の線条体解析. 第 51 回日本神経学会総会, 東京, 2010 年 5 月 20 日. (プログラム p75)

3. 奈良優子, 宮内ひとみ, 綾部啓子, 滝野直美, 中野今治, 村松慎一, 嶋崎久仁子：ALS 遺伝子治療用の血管内投与型AAVベクターの開発. 第51回日本神経学会総会, 東京, 2010 年 5 月 22 日. (プログラム p136)

4. Muramatsu S, Fujimoto K, Kato S, Asari S, Mizukami H, Ikeguchi K, Kawakami T, Urabe M, Kume A, Sato T, Watanabe E, Ozawa K and Nakano I: AADC gene therapy for Parkinson's disease:A phase I study. The Japan society of gene therapy's 16th annual meeting. Utsunomiya, July 1, 2010. (abstract p55)

5. Asari S, Fujimoto K, Kato S, Mizukami H, Ikeguchi K, Kawakami T, Urabe M, Kume A, Watanabe E, Sato T, Ozawa K, Nakano I and Muramatsu S : Positron emission tomography assessment of aromatic L-amino acid decarboxylase gene transfer in Parkinson's disease. The Japan society of gene therapy's 16th annual meeting. Utsunomiya, July 1, 2010. (abstract p166)

6. 浅利さやか, 藤本健一, 池口邦彦, 村松慎一, 中野今治, 齊藤順一, 佐藤俊彦, 宮内昭広 ：FMT-PET によるパーキンソン病の病態解析. 第 25 回日本大脳基底核研究会, 福島, 2010 年 8 月 1 日.

7. Tokuoka H, Muramatsu S, and Ichinose H: Compenensatory regulation of dopamine content in the nigro-striatal dopaminergic projection. Neuro2010, 神戸, 2010年9月2日.(神経化学 Vol .49 (No.2,3) p477, 2010)

8. Asari S, Fujimoto K, Kato S, Mizukami H, Ikeguchi K, Kawakami T, Urabe M, Kume A, Watanabe E, Sato T, Ozawa K, Nakano I and Muramatsu S : *In vivo* assessment of the aromatic L-amino acid decarboxylase gene expression by positron emission tomography in Parkinson's disease. Neuro2010, 神戸, 2010 年 9 月 2 日.(神経化学 Vol .49 (No.2,3) p484, 2010)

9. Popiel H A, Fujita H, Yamamoto K, Fujikake N, Muramatsu S, Toda T, Wada K and Nagai Y : Amelioration of neurological phenotypes and inclusion body formation in polyglutamine disease mice upon AAV5-mediated expression of aggregate inhibitor molecules. Neuro2010, 神戸, 2010 年 9 月 3 日.(神経化学 Vol.49 (No.2,3) p505, 2010)

10. 村松慎一：パーキンソン病の遺伝子・細胞治療. 第 20 回日本保健科学学会学術集会, 東京, 2010 年 10 月 9 日.(特別講演)(日本保健科学学会誌 Vol.13(1), p18)

11. 浅利さやか, 藤本健一, 池口邦彦, 村松慎一,中野今治, 齋藤順一, 佐藤俊彦, 宮内昭広：FMT-PET によるパーキンソン病の病態解析. Movement Disorder Society Japan 第 4 回学術集会, 京都, 2010 年 10 月 9 日. (抄録集 p98)

12. 村松慎一：神経変性疾患の遺伝子治療～AAV ベクターの応用～. 第 4 回 In vivo 実験医学シンポジウム～「In vivo 実験医学の今後の展望」～, 東京,

13. 2011 年 2 月 23 日.(招待講演)(プログラム p34-35)

H. 知的財産権の出願・登録状況

1. 特許

出願番号:2010-240581, 名称: 神経系細胞への遺伝子導入のためのアデノ随伴ウイルスビリオン, 出願人:自治医科大学, 出願日: 2010 年 10 月 27 日

2. 実用新案

なし

3. その他

なし

研究成果の刊行に関する一覧表

雑誌

発表者氏名	論文タイトル名	発表誌名	巻号	ページ	出版年
Matsumura, S., Shinoda, K., Yamada, M., Yokojima, S., Inoue, M., Ohnishi, T., Shimada, T., Kikuchi, K., Masui, D., Hashimoto, S., Sato, M., Ito, A., Akioka, M., Takagi, S., Nakamura, Y., Nemoto, K., Hasegawa, Y., Takamoto, H., Inoue, H., Nakamura, S., Nabeshima, Y., Teplow, D.B., Kinjo, M., and Hoshi, M.	**Two distinct amyloid β-PROTEIN (Aβ) assembly pathways leading to oligomers and fibrils identified by combined fluorescence correlation spectroscopy, morphology and toxicity analyses**	*J. Biol. Chem.*		in press	2011
Okada, S., Mizukami, S., **Kikuchi, K.**	Application of Stimuli-Responsive Polymer for Development of Novel MRI Probes.	*ChemBioChem*	1	785-787	2010
Watanabe, S., Mizukami, S., Hori, Y., **Kikuchi, K.**	Multicolor Protein Labeling in Living Cells Using Mutantβ-Lactamase-tag Technology.	*Bioconjugate Chem.*	21	2320-2326	2010
Sadhu, K.K., Mizukami, S., Watanabe, S., **Kikuchi, K.**	Turn-on Fluorescence Switch Involving Aggregation and Elimination Processes for β-Lactamase-Tag.	*Chem. Commun.*	46	7403-7405	2010
Mizukami, S., Hosoda, M., Satake, T., Okada, S., Hori, Y., Furuta, T., **Kikuchi, K.**	Photocontrolled Compound Release System Using Caged Antimicrobial Peptide.	*J. Am.Chem. Soc*	132	9524-9525	2010
Yoshimura, A., Mizukami, S., Hori, Y., Watanabe, S., **Kikuchi, K.**	Cell Surface Protein Labeling with Luminescent Nanoparticles via Biotinylation Using Mutant beta-Lactamase-tag Technology.	*ChemBioChem*	12	1031-1034	2011
Sadhu, K.K., Mizukami, S., Watanabe, S.,	Sequential Ordering Among Multicolor Fluorophores for Protein Labeling Facility via	*Mol. BioSyst.*	7	1766-1772	2011

Kikuchi, K.	Aggregation-elimination Based β-Lactam Probes.				
Mizukami, S., Matsushita, H., Takikawa, R., Sugihara, F., Shirakawa, M., **Kikuchi, K.**	^{19}F MRI Detection of β-Galactosidase Activity for Imaging of Gene Expression,	*Chem. Sci.*	2	in press	2011
Umetsu, Y., Taniguchi, R., Satomura, R., Goda, N., Ikegami, T., Furuse, M., Hiroaki, H.	^{1}H, ^{13}C, and ^{15}N resonance assignment of the first PDZ domain of mouse ZO-1.	Biomol. NMR Assign.		In press	2011
Umetsu, Y., Tenno, T., Goda, N., Shirakawa, M., Ikegami, T., Hiroaki, H.	Structural difference of vasoactive intestinal peptide (VIP) in two distinct membrane mimicking conditions.	*BBA-Proteins Proteomics*	1814	724-730	2011
Motono, C., Nakata, J., Koike, R., Shimizu, K., Shirota, M., Amemiya, T., Tomii, K., Nagano, N., Sakaya, N., Misoo, K., Sato, M., Kidera, A., Hiroaki, H., Shirai, T., Kinoshita, K., Noguchi, T., Ota, M.	SAHG, a comprehensive database of predicted structures of all human proteins.	Nucleic Acids Res.	39(suppl 1)	D487-D493	2010
Iwaya, N., Kuwahara, Y., Fujiwara, Y., Goda, N., Tenno, T., Akiyama, K., Mase, S., Tochio, H., Ikegami, T., Shirakawa, M., Hiroaki, H.	A common substrate recognition mode conserved between katanin p60 and VPS4 governs microtubule severing and membrane skeleton reorganization.	J Biol. Chem.	285	16822-16829	2010
Jee, J., Mizuno, T., Kamada, K., Tochio, H., Chiba, Y., Yanagi, K., Yasuda, G., Hiroaki, H., Hanaoka, F., Shirakawa, M.	Structure and mutagenesis studies of the C-terminal region of licensing factor Cdt1 enable the identification of key residues for binding to replicative helicase Mcm proteins.	J Biol. Chem.	285	15931-15940	2010
Krzyżosiak A, Szyszka-Niagolov M, Wietrzych M,	Retinoid X receptor gamma control of motivated behaviours involves dopaminergic signalling in mice.	Neuron	66(6)	908-920	2010

Gobaille S, Muramatsu S, Krężel W.					
Muramatsu S, Okuno T, Suzuki Y, Nakayama T, Kakiuchi T, Takino N, Iida A, Ono F, Terao K, Inoue N, Nakano I, Kondo Y and Tsukada H	A phase I study of aromatic L-amino acid decarboxylase gene therapy for Parkinson's disease.	Mol Ther	18(9)	731-1735	2010
Muramatsu S, Asari S, Fujimoto K, Ozawa K, Nakano I	Gene therapy for Parkinson's disease. Strategies for the local production of dopamine.	Gene Therapy & Regulation	5(1)	57-65	2010
Muramatsu S	The current status of gene therapy for Parkinson's disease,	Ann Neurosci	17(2)	92-95	2010

IV. 研究成果の刊行物・別刷り

THE JOURNAL OF BIOLOGICAL CHEMISTRY VOL. 286, NO. 13, pp. 11555–11562, April 1, 2011

Two Distinct Amyloid β-Protein (Aβ) Assembly Pathways Leading to Oligomers and Fibrils Identified by Combined Fluorescence Correlation Spectroscopy, Morphology, and Toxicity Analyses*[S]

Received for publication, September 6, 2010, and in revised form, January 23, 2011 Published, JBC Papers in Press, February 3, 2011, DOI 10.1074/jbc.M110.181313

Satoko Matsumura,[a1] Keiko Shinoda,[b1] Mayumi Yamada,[a1] Satoshi Yokojima,[b] Masafumi Inoue,[c] Takayuki Ohnishi,[c] Tetsuya Shimada,[d] Kazuya Kikuchi,[e] Dai Masui,[d] Shigeki Hashimoto,[f] Michio Sato,[a] Akane Ito,[a] Manami Akioka,[a] Shinsuke Takagi,[d] Yoshihiro Nakamura,[g] Kiyokazu Nemoto,[h] Yutaka Hasegawa,[i] Hisayoshi Takamoto,[i] Haruo Inoue,[d] Shinichiro Nakamura,[b] Yo-ichi Nabeshima,[c] David B. Teplow,[j] Masataka Kinjo,[k] and Minako Hoshi[a,c2]

From the [a]Mitsubishi Kagaku Institute of Life Sciences, Tokyo 194-8511, Japan, [b]Mitsubishi Chemical Group Science and Technology Research Center, Inc., Yokohama 227-8502, Japan, [c]Kyoto University, Kyoto 606-8501, Japan, [d]Tokyo Metropolitan University, Tokyo 192-0397, Japan, [e]Osaka University, Osaka 565-0871, Japan, [f]Tokyo University of Science, Hokkaido 049-3514, Japan, [g]Nagoya Institute of Technology, Aichi 466-8555, Japan, [h]Chibadai Inohana Innovation Plaza, Chiba 260-0856, Japan, [i]Hamamatsu Photonics K.K., Shizuoka 438-0193, Japan, [j]University of California, Los Angeles, California 90095, and [k]Hokkaido University, Sapporo 001-0021, Japan

Nonfibrillar assemblies of amyloid β-protein (Aβ) are considered to play primary roles in Alzheimer disease (AD). Elucidating the assembly pathways of these specific aggregates is essential for understanding disease pathogenesis and developing knowledge-based therapies. However, these assemblies cannot be monitored *in vivo*, and there has been no reliable *in vitro* monitoring method at low protein concentration. We have developed a highly sensitive *in vitro* monitoring method using fluorescence correlation spectroscopy (FCS) combined with transmission electron microscopy (TEM) and toxicity assays. Using Aβ labeled at the N terminus or Lys^{16}, we uncovered two distinct assembly pathways. One leads to highly toxic 10–15-nm spherical Aβ assemblies, termed amylospheroids (ASPDs). The other leads to fibrils. The first step in ASPD formation is trimerization. ASPDs of ~330 kDa in mass form from these trimers after 5 h of slow rotation. Up to at least 24 h, ASPDs remain the dominant structures in assembly reactions. Neurotoxicity studies reveal that the most toxic ASPDs are ~128 kDa (~32-mers). In contrast, fibrillogenesis begins with dimer formation and then proceeds to formation of 15–40-nm spherical intermediates, from which fibrils originate after 15 h. Unlike ASPD formation, the Lys^{16}-labeled peptide disturbed fibril formation because the Aβ$^{16-20}$ region is critical for this final step. These differences in the assembly pathways clearly indicated that ASPDs are not fibril precursors. The method we have developed should facilitate identifying Aβ assembly steps at which inhibition may be beneficial.

Conversion of disease-specific amyloid proteins from the native forms into fibrillar assemblies is a common feature of a wide range of human pathologies, including neurodegenerative diseases such as AD,[3] Parkinson disease, prion diseases, and the polyglutamine diseases (1–5). On the other hand, smaller, nonfibrillar assemblies, which might be early precursors in fibrillogenesis, have recently been considered to be more proximate mediators of neurotoxicity (1–5). However, it is unclear whether these originate from a linear process or a series of parallel processes involving different intermediates. Thus, ordering the assembly pathway(s) is essential for understanding disease pathogenesis and developing rational therapeutics, as inhibiting inappropriate step(s) could increase the level of the toxic assemblies (2, 5).

In AD, various forms of toxic Aβ assemblies, ranging in mass from dimers to multimers of ~1 MDa, have been reported (6–14). These assemblies may play the key role in AD pathogenesis by causing synaptic impairment (12, 13, 15–17). Indeed, Aβ dimers that induce synaptic impairment and not neuronal loss have been reported to be isolated from AD brains (18). In contrast, the molecular natures of the Aβ assemblies that directly cause neuronal loss in human AD remain to be elucidated. Because neuronal loss causes cognitive deterioration in AD patients (19), we sought to isolate such Aβ assemblies *in vivo*. As a first step, we prepared highly toxic 10–15-nm spherical Aβ assemblies termed ASPDs using an *in vitro* assembly

* This work was supported by grants from the Ministry of Health, Labor and Welfare (Research on Nanotechnical Medical) (to M. H.), Special Coordination Funds for Promoting Science and Technology from the Ministry of Education, Culture, Sports, Science, and Technology (to K. K. and M. H.), the New Energy and Industrial Technology Development Organization (Translational Research Promotion Project) (to M. H.), and the Jim Easton Consortium for Alzheimer's Drug Discovery and Biomarkers (to D. B. T.).

[S] The on-line version of this article (available at http://www.jbc.org) contains supplemental "Experimental Procedures," equations, Table S1, Figs. S1–S8, and additional references.

[1] These authors contributed equally to the work.

[2] To whom correspondence should be addressed: Yoshidakonoecho, Sakyo-ku, Kyoto 606-8501, Japan. Tel.: 81-75-7534683; Fax: 81-75-7534676; E-mail: minhoshi@lmls.med.kyoto-u.ac.jp.

[3] The abbreviations used are: AD, Alzheimer disease; Aβ, amyloid β-protein; FCS, fluorescence correlation spectroscopy; TEM, transmission electron microscopy; ASPD, amylospheroid; ADDLs, Aβ-diffusible ligands; TMR, tetramethylrhodamine; ha, hamster monoclonal; PBS, Dulbecco's phosphate-buffered saline without Ca^{2+} and Mg^{2+}; IP, immunoprecipitation.

system (10). ASPDs are not fibril intermediates because they are not incorporated into mature fibrils and continue to exist after fibril formation ceases (5, 10). They also differ from protofibrils and Aβ-derived diffusible ligands (ADDLs) in morphology and size (10) (see reviews in Refs. 5 and 20)). Recently, we have produced ASPD-specific antibodies and used them to selectively immunoisolate highly neurotoxic ASPDs from human AD brains (21), strengthening the hypothesis that ASPDs are effectors of neurodegeneration *in situ* in humans. We also found that ASPD concentration correlated with the pathological severity of AD (21). These findings suggest that native ASPDs might be a candidate for Aβ assemblies that directly cause neuronal loss in human AD brains. The immunoreactivity profile of ASPD-specific antibodies in comparison to that of anti-Aβ antibodies or of an anti-oligomer A11 antibody suggests that ASPDs are structurally distinct from dimers, ADDLs, and A11-reactive entities (21). Taken together, data extant suggest that distinct types of Aβ assemblies, with distinct neurotoxic activities, exist in the AD brain. Therefore, elucidation of the assembly state-neurotoxicity relationships of these assemblies is important for understanding AD pathogenesis.

Here, we use combined FCS, TEM, and toxicity analyses to address these issues and to provide a highly sensitive and reliable method for *in situ* monitoring of the assembly process. At present, the assembly process cannot be monitored directly *in vivo* and much higher sensitivity is required for reliably monitoring *in vitro* formation of nonfibrillar Aβ assemblies, which occurs at low protein concentration (5, 20, 22–25). Our approach should therefore be useful in studies of other amyloid proteins.

FCS involves autocorrelation of fluctuations of fluorescence intensity, which gives the average number and average diffusion time (*i.e.* molecular size) of fluorescent molecules as they diffuse through an illuminated volume (26). We employed FCS because FCS provides the highest sensitivity for detecting small assemblies in dilute solutions among available analytical techniques (small angle x-ray diffraction, ultracentrifugation, laser light scattering, etc.). In addition, FCS does not require physical separation of metastable assemblies, and its noninvasive character allows monitoring without perturbation of monomer-nonfibrillar assembly-fibril equilibria (27–29). Although FCS has been employed to detect Aβ aggregates in cerebrospinal fluid of AD patients (30) and the formation of large (>10^4 kDa) fibrillar assemblies from $A\beta^{1-40}$ *in vitro* (29, 31), little is known about the formation of neurotoxic nonfibrillar Aβ assemblies. Here, by using combined FCS, TEM, and toxicity analyses, we uncovered two distinct assembly pathways, one leading to ASPDs and the other to fibrils. We also determined the mass (128 ± 44 kDa) and height (7.2 ± 2.6 nm) of the most toxic ASPDs. The observed differences in the assembly pathways clearly indicated that ASPDs are not fibril precuorsors.

EXPERIMENTAL PROCEDURES

Materials—ASPD-specific antibodies, a rabbit polyclonal rpASD1 ($K_d \approx 5$ pM) and a hamster monoclonal haASD1 ($K_d \approx 0.5$ pM), have been produced in our laboratory and recognize epitopes distinct from those present on dimers, A11 antibody-reactive 12-mers, or fibrils (21). The characteristics of these ASPD tertiary structure-dependent antibodies are summarized in supplemental Table S1.

Sample Preparations—Fluorescent probes, $A\beta^{1-40}$ site-specifically labeled with tetramethylrhodamine (TMR) either at the N terminus (NTR) or Lys16 (K16TR), were synthesized (supplemental "Experimental Procedures"). ASPDs were prepared *in vitro* from 50 μM solutions of $A\beta^{1-42}$ (with or without 0.1 μM NTR or K16TR; a probe ratio of 1/500) in F12 buffer without riboflavine, L-glutamine, and phenol red by slowly rotating the solutions at 4 °C for 16.5 h (10). Their quality was confirmed by dot blotting, TEM, and toxicity assays. Spherical assemblies 10–15 nm in diameter, with rare fibril-like structures, were usually produced as major components (10). Fibrils were prepared from 100 μM solutions of $A\beta^{1-40}$ (with or without 0.1 μM NTR or K16TR; a probe ratio of 1/1000) in 0.5× Dulbecco's phosphate-buffered saline without Ca^{2+} and Mg^{2+} (PBS) at pH 3.5 by slowly rotating the solutions at 4 °C for 2 days. Fibrils without ASPDs were detected by TEM. Aβ concentration of each preparation was determined by quantitative amino acid analysis (Waters AccQ-Tag system) (10).

FCS—FCS was performed with a confocal volume element of 0.3 femtoliters using a preproduction prototype apparatus (Hamamatsu Photonics K.K.). The fluorescence intensity fluctuations were detected using a photomultiplier tube, and the autocorrelation function was calculated using a digital correlator (Fig. 1*A*; see also supplemental "Experimental Procedures"). Each sample (20 μl) was measured at room temperature for 3 s × 10 times using free rhodamine 6G (479 Da in mass, 2.8×10^{-10} m^2 s^{-1} in the diffusion coefficient (*D*)) or Alexa Fluor 532 C5 maleimide (813 Da, 2.8×10^{-10} m^2 s^{-1}) as reference dyes.

FCS Data Evaluation—At the onset of the assembly process, Aβ solutions mainly contain rapidly diffusing Aβ assemblies ranging in mass from monomers to trimers. Some other assemblies may also be present, but their concentrations are unpredictable. Therefore, the constrained regularization program CONTIN (32, 33), combined with least-squares fitting, was utilized to determine the distribution of the diffusion times so that the mass of the rapidly diffusing Aβ assemblies fitted the dimer/trimer range (8~15 kDa), without any prior assumption about the number of the assembly types in solutions. From the determined distributions, the relative abundance and diffusion time of each assembly were calculated. By comparing the diffusion time of each assembly with that of reference dyes with known mass and diffusion coefficient, the mass (for spherical assemblies such as ASPDs) or the diffusion coefficient (*D*) (for nonspherical assemblies such as fibrils) was determined (supplemental Fig. S3). The details are described in the supplemental "Experimental Procedures."

In FCS, the contribution of each component to the correlation curve is related to both its relative abundance and brightness (34). If all components have equal brightness, the relative abundance of each assembly can be obtained directly from the distribution of assembly diffusion time. This is true for ASPDs and early fibril intermediates, but not for fibrils containing more than one fluorophore. In the latter case, a rough estimate of the relative abundance of the fibrils was obtained from the distribution of the diffusion time (for details, see "*In Situ* Monitoring of Fibril Formation" under "Results"). To confirm the estimates thus obtained,

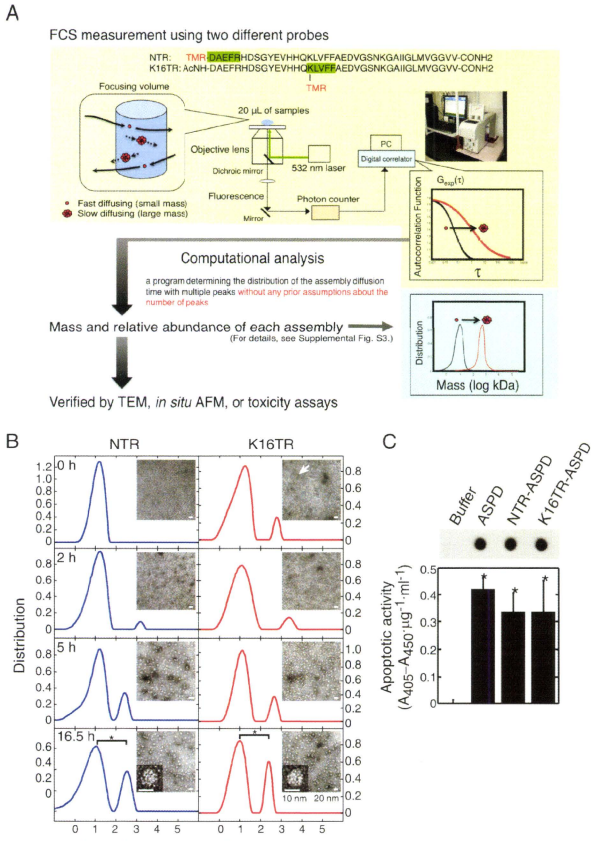

FIGURE 1. **Time course of ASPD formation.** *A*, schematic representation of FCS-based method. *B*, time course of ASPD formation. At the indicated time, aliquots were examined by TEM (*inset*) and FCS ($n = 10$). The distribution of assembly mass is shown (*, $p < 0.005$ by Scheffé post hoc test compared with the fast-diffusing assembly). Each distribution is normalized so that the total area becomes 1 (as described under "Experimental Procedures"). An *arrow* in TEM data indicates not-yet-dissolved amorphous aggregates. *C*, characterization of ASPDs formed with or without probes in dot blotting (1 pmol/dot using 0.04 μg/ml ASPD-specific rpASD1 antibody) or specific apoptotic activity against rat primary septal neuronal cultures, determined by monitoring cytoplasmic histone-associated DNA fragments, and normalized by the amount of Aβ present (mean ± S.D.; Games-Howell post hoc test. *, $p < 0.005$, $n = 6$; see supplemental "Experimental Procedures").

mature fibrils were separated in the retentate fractions of 0.1-μm filters (confirmed using TEM), and their amount was directly obtained from the fluorescence count using a fluorometer (Twinkle LB970; Berthold Technologies GmbH).

Other Methods—Immunoprecipitation (IP), TEM, fluid-phase imaging of ASPDs by atomic force microscopy, toxicity assays, and statistics are described in the supplemental "Experimental Procedures."

RESULTS

Fluorescent Probes for FCS Measurements and Program for FCS Analysis—To monitor ASPD formation by FCS, we chemically synthesized fluorescent probes by labeling TMR site-specifically either at the N terminus (termed NTR) or at Lys^{16} (termed K16TR) of $A\beta^{1-40}$ (Fig. 1*A*). We consider TMR labeling at these sites to minimally affect ASPD formation because

excess $A\beta^{1-5}$ (DAEFR) or $A\beta^{16-20}$ (KLVFF) had no effect on ASPD formation (supplemental Fig. S1), suggesting that amino acid residues around $A\beta^{1-5}$ or $A\beta^{16-20}$ are not involved in ASPD formation.

FCS was performed using a preproduction prototype apparatus (Hamamatsu Photonics K.K.) at 100 μW optimum laser output power (supplemental Fig. S2). From FCS data, the relative abundance (%) and diffusion time of each Aβ assembly were obtained using CONTIN (32, 33) combined with least-squares fitting (Fig. 1*A*; see supplemental "Experimental Procedures"). By comparing the diffusion time of each assembly with those of reference dyes (rhodamine 6G and Alexa Fluor 532) with known mass and diffusion coefficient, either the assembly mass (for spherical assemblies such as ASPDs) or diffusion coefficient (*D*) (for nonspherical assemblies such as fibrils) was determined (supplemental Fig. S3, *A* and *B*).

First, we examined the masses of the probes by FCS. The average mass values of the probes, freshly dissolved at 0.1 μM in 0.5× PBS, were calculated to be 7.9 kDa (NTR) and 8.6 kDa (K16TR), respectively ($n = 5$), assuming they behave as spherical structures. Thus, these probes (4.8 kDa nominal mass) behave as dimers, like unlabeled $A\beta^{1-40}$ (35), and should be available for incorporation into ASPDs during assembly. The result validates the accuracy of our FCS-based analytical method.

In Situ Monitoring of ASPD Formation—Next, we examined whether ASPDs were formed in the presence of the probes. Consistent with our study using unlabeled $A\beta^{1-42}$ (10), TEM revealed the formation of 10–15-nm ASPDs in the presence of NTR or K16TR at various ratios (1/500~1/10 of total Aβ; 16.5 h in Fig. 1*B*, *inset*). FCS detected ASPD-sized structures in the range of 100–1000 kDa (16.5 h in Fig. 1*B*) (10) even at a 1/500 probe ratio. NTR- or K16TR-labeled ASPDs were indistinguishable from unlabeled ASPDs in immunoreactivity to anti-ASPD antibodies and in neurotoxicity to rat primary neuronal cultures (Fig. 1*C*). Accordingly, we set the probe ratio at 1/500 for subsequent experiments. Because the mass of ASPDs does not exceed 669 kDa (*i.e.* ~148-mer) (21), at 1/500 probe ratio, assemblies will contain a maximum of one fluorophore per assembly, so they will have equal brightness. This means that we can obtain the relative abundance of each assembly directly from the distribution of assembly diffusion time determined by CONTIN (see "Experimental Procedures").

We then followed time-dependent changes in Aβ assembly state simultaneously using TEM and FCS (Fig. 1*A*). As shown previously (10), during up to 2 h of slow rotation, TEM detected few structures except for occasional amorphous structure (Fig. 1*B*, *arrow* at 0 h in *inset*). During this initial phase of ASPD formation, up to 2 h, Aβ trimers (12.7 ± 1.8 kDa, 92%, $n = 8$) predominated (Fig. 1*B*). This means the first step in ASPD formation involves trimerization. Besides trimers, FCS also detected small amounts of large assemblies with varying mass and relative abundance (for time 0, 10^2~10^7 kDa in mass, 8.4 ± 11%; for 2 h, 10^2~10^4 kDa, 11.3 ± 7.2%; $n = 8$) (supplemental Fig. S4). This is consistent with the observation of low numbers of cloud-like uranyl acetate staining structures (*dotted line* in supplemental Fig. S4, *inset*), distinct from the staining of buffer-derived salts, up to 2 h in TEM. We speculate that these large species are metastable and therefore may be destroyed during sample preparation for TEM. Although it is unclear whether these species are intermediates of ASPDs, it is noteworthy that neither the cloud-like structures nor the large species with such variety in mass and relative abundance were absent at the onset of fibril formation (see "*In Situ* Monitoring of Fibril Formation"; see Fig. 3). After that, ASPDs appeared at 5 h of slow rotation. At this time, 5–20-nm spherical structures, mainly 10–15-nm ASPD-sized spheres, were observed (Fig. 1*B*, *inset*). ASPDs remained as the dominant structures from 5 h until at least 24 h (Fig. 1*B*, *inset*). In accordance with TEM observations, FCS detected an ASPD-sized assembly of 10^2 ~ 10^3 kDa at 5 h, and its amount was increased at 16.5 h (Fig. 1*B* and supplemental Fig. S4). Its mass was 330 ± 58 kDa (24 ± 7.7%, $n = 5$), in good agreement with that of ASPDs (~158–669 kDa) previously estimated from glycerol-gradient sedimentation assays (5, 10). Thus, we conclude we could monitor ASPD formation continuously and quantitatively using FCS. The two probes gave essentially identical results (Fig. 1*B*).

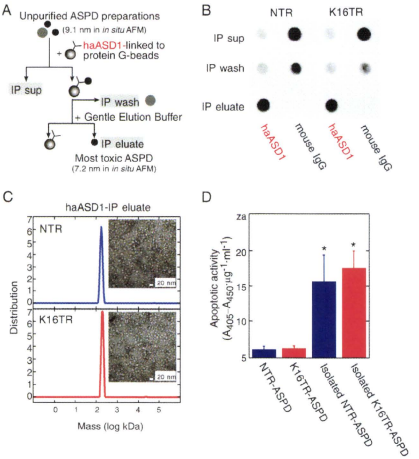

FIGURE 2. **Isolation of the most toxic ASPD fraction.** *A*, method for IP. *B*, dot blotting (using 0.04 μg/ml rpASD1) of IP supernatant (*sup*), wash, and eluate fractions. *C*, the isolated ASPDs in haASD1-IP eluates examined by TEM (*Inset*) and FCS ($n = 10$). The distribution is normalized as in Fig. 1*B*. ASPDs were undetectable in mouse IgG-IP eluates using TEM or FCS (data not shown). *D*, specific apoptotic activities of the isolated ASPDs and unpurified ASPDs were examined as in Fig. 1*C* (mean ± S.D.; Games-Howell post hoc test; *, $p < 0.001$, $n = 6$).

Mass and Height of Isolated ASPDs—We recently produced ASPD-specific antibodies (supplemental Table S1) (21) and used them to selectively immunoisolate ASPDs from AD brain extracts without affecting ASPD structure or neurotoxicity (21). With this method (Fig. 2*A*), we immunoisolated the most toxic fraction of ASPDs from unpurified ASPD preparations and determined the mass using our FCS method. Large amounts of 10–15-nm ASPDs were detected only in IP eluates of a monoclonal ASPD-specific haASD1 antibody, whereas ASPDs were undetectable in IP eluates of normal mouse IgG

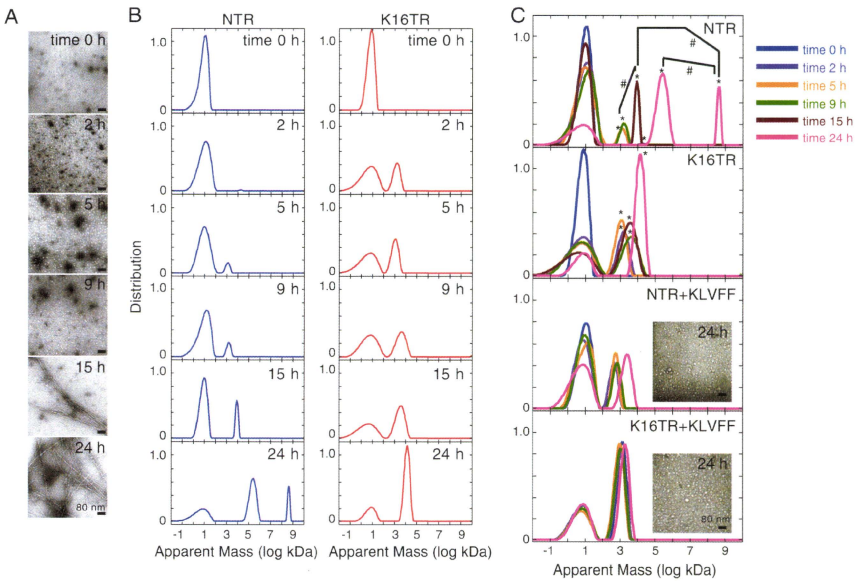

FIGURE 3. **Time course of fibril formation.** *A* and *B*, fibrils were formed from 100 μM solutions of $A\beta^{1-40}$ with 0.1 μM NTR or K16TR at pH 3.5. At the indicated time, aliquots were examined by TEM (*A*) and FCS ($n = 5$) (*B*). As fibrillogenesis proceeded essentially in the same way with or without probes, representative TEM images of fibrils with NTR are shown. The normalized distribution of apparent assembly mass (see supplemental Fig. S7 for diffusion coefficient) is shown, as in Fig. 1*B*. *C*, at the onset of fibril formation, a 10-fold molar excess of $A\beta^{16-20}$ (KLVFF) was added to the $A\beta^{1-40}$ solutions, and analyses using TEM (*inset*) and FCS were performed as above (*, $p < 0.005$ by Scheffé post hoc test compared with the fast-diffusing assembly corresponding to dimers; #, $p < 0.005$ by Scheffé post hoc test). The probability distribution is normalized as in Fig. 1*B*.

(Fig. 2, *B* and *C*, *inset*). In accordance with this, 97% of the fluorescent species in haASD1-IP eluates detected by FCS was ASPD-sized assemblies of 128 ± 44 kDa ($n = 6$) (Fig. 2*C*). The IP process mostly eliminated Aβ dimers (9.4 ± 4.0 kDa) (Fig. 2*C*), which had been a major component before IP (76%, $n = 5$, 16.5 h in Fig. 1*B*). The neurotoxicity of the purified ASPDs to rat primary neuronal cultures was >10 times greater than that of the unpurified ASPD preparations (Fig. 2*D* and supplemental Fig. S5). These data collectively indicated that the most toxic ASPDs were concentrated by the IP procedures. Their mass estimated from FCS analysis was in good agreement with our previous sedimentation results, which indicated that the highest toxicity exists in the fraction at the migration position of 158-kDa aldolase (10, 21). The most toxic ASPDs (128 ± 44 kDa; ~32-mers) were smaller in mass than the unpurified ASPDs (330 ± 58 kDa; compare Fig. 2*C* with 16.5 h in Fig. 1*B*). Consistent with these data, *in situ* atomic force microscopy imaging in physiological solutions (10) revealed that the average height of the most toxic ASPDs (7.2 ± 2.6 nm, 94%, supplemental Fig. S6) was smaller than that of the unpurified ASPDs (9.1 ± 2.0 nm (10)). We thus have succeeded in determining the mass and height of the most toxic ASPDs for the first time.

In Situ Monitoring of Fibril Formation—We next monitored fibril formation (supplemental Fig. S3B). We used acidic solutions because fibrils are well formed from 100 μM $A\beta^{1-40}$ at pH 3.5 (36), whereas ASPDs are hardly formed (24 h in Fig. 3*A*). Because fibrils contain higher numbers of Aβ monomers than ASPDs (10), we set the probe ratio for fibrils at 1/1000. As with ASPDs, if all components have equal brightness, the relative abundance of each assembly can be obtained from the distribution of assembly diffusion times determined by CONTIN. This is true for early assemblies before 15 h (< 5,000 kDa) that will contain a maximum of one fluorophore per assembly at 1/1000 probe ratio. However, this might not be the case for late stage assemblies (after 15 h), which include very large assemblies (probably mature fibrils) with more than one fluorophore per assembly (Fig. 3); here, as the contribution of a component to the FCS correlation curve scales with the brightness squared, the fraction of brighter component will be overestimated (34). The problem is that the number of fluorophores per fibril (*i.e.* fibril brightness) cannot be determined, because fibrils exist over a wide mass range. Furthermore, fibril formation may alter the fluorophore quantum yield (37). Therefore, a rough estimate of fibril amount was obtained from the distribution of

assembly diffusion times and was confirmed by separating the mature fibrils in retentate fractions on 0.1-μm filters and by directly measuring their fluorescence.

As with ASPDs, time-dependent changes in Aβ assembly state were monitored simultaneously using TEM and FCS (Fig. 3). At the onset of slow rotation, amorphous structures incorporating small globular structures (<3 nm) were occasionally detected in trace amounts with TEM (Fig. 3*A*). At 2 h, as reported previously (14), 15–40-nm spherical intermediates (larger than 10–15-nm ASPDs) appeared and increased until 5 h (Fig. 3*A*). Then, with the formation of short fibril-like structures, these spherical intermediates decreased at 9 h and were no longer detectable at 15 h (Fig. 3*A*). Mature fibrils appeared at 15 h, and their amount was markedly increased at 24 h. Subsequently, these fibrils grew into meshwork-like or bundled fibrils (Fig. 3*A*). These morphological changes generally occurred in this sequence, irrespective of the presence or absence of probes, although the size and morphology of mature fibrils varied somewhat among preparations.

TEM observations confirmed that the presence of either probe at 1/1000 did not affect overall fibrillogenesis (Fig. 3*A*). However, the two probes gave different FCS results at 24 h (Fig. 3*B*). To illustrate the time-dependent size changes, we show the diffusion coefficient (supplemental Fig. S7) and apparent mass (Fig. 3) of each structure both for spherical structures (5 h in Fig. 3*A*) and nonspherical structures (15 and 24 h in Fig. 3*A*). Unlike ASPD formation, at the onset of fibril formation, Aβ dimers (9.2 ± 1.7 kDa, 85% at time 0, $1.4 \pm 0.2 \times 10^{-10}$ m^2s^{-1}, $n = 6$) were the dominant species (Fig. 3*B*), which decreased to 41% at 24 h. Consistent with the TEM results, large aggregates of ~10^3 kDa were occasionally detected by FCS at time 0. At 2 h, Aβ assemblies of ~2910 kDa in average mass appeared and remained detectable up to 9 h (29%, $2.2 \pm 0.7 \times 10^{-11}$ m^2s^{-1}, $n = 18$; see NTR and K16TR in upper two panels in Fig. 3*C*). Their average masses likely correspond to the 15–40-nm spherical intermediates (5 h in Fig. 3*A*). At 15 h, consistent with their disappearance in TEM (Fig. 3*A*), they were hardly detectable with FCS, and other Aβ assemblies of 5.4×10^3 kDa in apparent mass, a slightly larger than the 15–40-nm intermediates, appeared (roughly 38%, $1.6 \pm 0.4 \times 10^{-11}$ m^2 s^{-1}, $n = 6$; Fig. 3*B*). Although the two probes, NTR and K16TR, behaved similarly up to 15 h, they gave different results at 24 h. NTR detected two kinds of Aβ assemblies, a very large Aβ assembly of 1.2×10^5 kDa in apparent mass (roughly 45%, $0.7 \pm 0.4 \times 10^{-11}$ m^2 s^{-1}, $n = 3$) and another much larger Aβ assembly of 3.9×10^9 kDa in apparent mass (roughly 7%, $1.9 \pm 0.9 \times 10^{-13}$ m^2 s^{-1}, $n = 3$) (Fig. 3*B*). However, K16TR only detected the former very large Aβ assembly of 1.4×10^4 kDa in apparent mass (roughly 64%, $1.3 \pm 0.7 \times 10^{-11}$ m^2 s^{-1}, $n = 3$), but failed to detect the latter huge Aβ assembly (Fig. 3*B*). As described above, to confirm the estimates at 15 and 24 h, the fibril amount was directly obtained by filtration using 0.1-μm filters, followed by counting of fluorescence intensity. The fibril amounts in the 0.10-μm retentates were 29 ± 7% (NTR) and 36 ± 3% (K16TR) at 15 h, and 74 ± 7% (NTR) and 61 ± 6% (K16TR) at 24 h ($n = 5$; supplemental Fig. S8). These data seem consistent with the FCS results (38% at 15 h ($n = 6$) and 52% for NTR and 64% for K16TR at 24 h ($n = 3$)) (Fig. 3*B*), suggesting that the fibril amount can be estimated using FCS.

As for the difference between NTR and K16TR at 24 h, we speculate that TMR introduced at Lys^{16} disturbed incorporation of K16TR into mature fibrils, because the 16–20 region of Aβ is known to be critical for Aβ self-association and subsequent fibril formation (38). To examine this hypothesis, we added excess $Aβ^{16-20}$ (KLVFF) at the onset of Aβ assembly. In TEM and FCS analyses (Fig. 3*C*), 15–40-nm spherical intermediates that had disappeared at 15 h without $Aβ^{16-20}$ (Fig. 3, *A* and *B*) remained as the dominant structures in the presence of excess $Aβ^{16-20}$, up to 24 h (Fig. 3*C*, *inset*). NTR and K16TR both detected these spherical intermediates even at 24 h (2280 kDa, for $2.2 \pm 0.2 \times 10^{-11}$ m^2 s^{-1} for NTR, 3370 kDa, $1.9 \pm 0.3 \times 10^{-11}$ m^2 s^{-1} for K16TR, $n = 3$, Fig. 3*C* and supplemental Fig. S7). This result indicated that $Aβ^{16-20}$ did not prevent assembly of Aβ dimers into spherical intermediates but blocked conversion of the latter into fibrils.

DISCUSSION

A large body of evidence supports the hypothesis that nonfibrillar Aβ assemblies play causative roles in AD (3, 5, 20, 22–25). Accordingly, Aβ assemblies other than fibrils have recently been proposed as therapeutic targets (39). However, Aβ monomers develop into various nonfibrillar Aβ assemblies differing in size and toxicity, which might represent distinct structural variants (5, 20, 24, 40). It is not clear whether and how these different types of assemblies are related to each other or indeed how they contribute to AD pathogenesis.

To elucidate the neurotoxic molecular entities responsible for AD pathogenesis, several approaches have been employed to reveal the formation of nonfibrillar Aβ assemblies *in vitro*. For example, studies using HPLC multiangle laser light scattering analysis (41) determined the size of certain forms of nonfibrillar Aβ assemblies. Studies using a UV-cross-linking method (42) or limited proteolysis with mass analysis (43) elucidated the roles of various amino acid residues in the formation of nonfibrillar Aβ assemblies, and solid-state NMR analysis revealed conformational changes in the early stage of fibril formation (14). Interestingly, in the case of cross-linked Aβ oligomers, higher order oligomers have stronger neurotoxicity (44). These studies and others together suggest that assembly may not be a linear process but may be the result of a series of multiple processes involving intermediates from side paths (5). However, these approaches could not follow the continuous changes of assembly state in solution and the assembly state-neurotoxicity relationship largely remained to be uncovered.

Here, we have developed a highly sensitive *in vitro* monitoring method using combined FCS, TEM, and toxicity analyses. Applying this method to Aβ labeled with TMR at the N terminus or Lys^{16}, we uncovered two distinct assembly pathways, one leading to highly toxic 10–15-nm spherical Aβ assemblies termed ASPDs (10), which we showed to exist *in vivo* (21), and the other to fibrils. The first step in ASPD formation is trimerization. ASPDs of ~330 kDa in mass originate from these trimers after 5 h of slow rotation (Fig. 1*B*). At least until 24 h, ASPDs remained the dominant structures in these reactions. Previously, we reported that ASPDs are formed from 50 μM

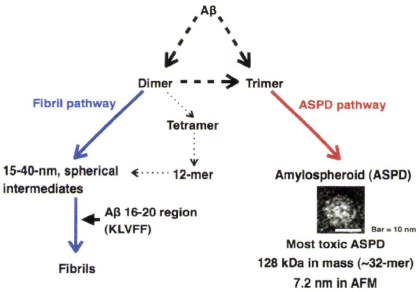

FIGURE 4. **Two distinct Aβ assembly pathways, one leading to ASPDs (*red*) and the other to fibrils (*blue*).** The first step in ASPDs formation is trimerization (Fig. 1), whereas the pathway to fibrils begins with dimers, which further assemble into 15–40-nm spherical intermediates, eventually leading to fibrils (Fig. 3*B*). The $A\beta^{16-20}$ region is critical for intermediate conversion into fibrils (Fig. 3*C*), but not for ASPD formation (supplemental Fig. S1). Although the assembly pathway to 12-mers is unknown, tetramers might serve as a precursor of 12-mers (45); if this is so, the assembly pathway to 12-mers (*dotted line*) differs at the initial step from that of ASPDs.

$A\beta^{1-42}$ within 14 h during slow rotation (10). With the present method, we could thus more easily and accurately monitor ASPD formation, as well as detect ASPDs themselves. Indeed, we found that the most toxic ASPDs are ~128 kDa in mass (~32-mers) (Fig. 2 and supplemental Fig. S5) and are 7.2 nm in height (supplemental Fig. S6).

Our previous data have strongly suggested that ASPDs have a distinct tertiary structure from other assemblies (21). Therefore, we were interested in whether or not ASPDs share building blocks with these assemblies. With respect to dimers (18), we found that they clearly are not building blocks *per se* because the initial step in ASPD formation is trimerization (Fig. 1*B*). We could not detect 12-mers during ASPD formation (supplemental Fig. S4). This suggests that 12-mers are not precursors of ASPDs. Although the assembly pathway to 12-mers is unknown, ion mobility-mass spectrometry studies have shown that tetramers might serve as a precursor of 12-mers (45), indicating that the assembly pathway to 12-mers may differ at the initial step from that of ASPDs. These results collectively demonstrated that the assembly pathway to ASPDs is distinct from those leading to dimers and to 12-mers. We propose a scheme of the assembly pathways based on these findings (Fig. 4).

In contrast to ASPD formation, the first step leading to fibrils consists in the assembly of Aβ monomers into dimers, which further assemble into 15–40-nm spherical intermediates, eventually leading to fibrils (blue arrows in Fig. 4). Although the $A\beta^{16-20}$ region is not involved in ASPD formation (supplemental Fig. S1), we found that this region is critical for conversion of the spherical intermediates to fibrils because probe labeling at Lys^{16} was found to disturb fibrillogenesis (Fig. 3*C*). Excess amounts of the $A\beta^{16-20}$ (KLVFF) peptide in fibril formation reactions inhibited the process, supporting this conclusion (Fig. 3*C*). As for 12-mers, we could not detect them as a single peak during fibril formation (Fig. 3*B*), which suggests that even though 12-mer formation appears to begin with dimer formation (45), the 12-mers do not directly serve as a primary fibril precursor (Fig. 4). This view is consistent with other studies showing that 12-mers are semistable structures that do not readily form fibrils (12), and it would likely take a slow transformation process for them to rearrange into fibrils (45). Of relevance to the role of dimers in fibrillogenesis are data recently published by the Walsh and co-workers (46) that show that dimers themselves are inert with respect to neurotoxicity but that their further assembly produces higher order toxic prefibrillar assemblies. Consistently with this, dimers in AD brains have been reported to be contained in amyloid cores as insoluble reservoirs that do not readily dissociate (18).

Previously, we have shown that both $A\beta^{1-40}$ and $A\beta^{1-42}$ form ASPDs of ~158–669 kDa in sedimentation assays, and among them, the highest toxicity exists in the fraction at the migration position of 158 kDa (aldolase) (10, 21). Epitope analysis of ASPD-specific antibodies has also suggested that $A\beta^{1-40}$ and $A\beta^{1-42}$ ASPDs share the same tertiary structures because essentially the same results are obtained in inhibition studies of ASPD-specific antibodies through the binding to either $A\beta^{1-40}$ or $A\beta^{1-42}$ ASPDs of pentapeptides derived from Aβ (21). However, there exists a critical difference between $A\beta^{1-40}$ and $A\beta^{1-42}$ in the rate and speed of ASPD formation. $A\beta^{1-42}$ ASPDs are formed more rapidly, after 5 h of incubation, and in greater quantities (24%). They induce neurodegeneration at lower concentration (~0.35 nM) and exhibit ~100-fold higher toxicity than $A\beta^{1-40}$ ASPDs (10). In contrast, $A\beta^{1-40}$ forms ASPDs after 3 days of incubation, but in lesser amounts (5% on average) than does $A\beta^{1-42}$ (10). These observations are consistent with the general consensus that $A\beta^{1-42}$ is more toxic than $A\beta^{1-40}$. Interestingly, we found that the first step to $A\beta^{1-40}$ ASPDs also consists in the assembly of $A\beta^{1-40}$ monomers into trimers (12.7 ± 0.4 kDa, 93%, $n = 4$; data not shown). Although $A\beta^{1-40}$ seemingly behaves as trimers in FCS, we speculate that, probably because of the absence of the stabilizing influence of the hydrophobic carboxyl terminus, $A\beta^{1-40}$ trimers are more unstable than $A\beta^{1-42}$ trimers and therefore less likely to form ASPDs. This view is supported by other studies using different analytical methods, including SDS-PAGE, ion mobility-mass spectroscopy, and size exclusion spectroscopy (45, 47, 48), all of which have indicated the absence of trimers/tetramers in $A\beta^{1-40}$. Certain differences in the initial folded structures and properties between $A\beta^{1-40}$ and $A\beta^{1-42}$ might be reflected in the differences in their ability to form higher order assemblies (45, 47, 48). Although the conformation adopted by Aβ within the nonfibrillar Aβ assemblies is not known, a β-hairpin has recently been reported to be a building block of toxic Aβ assemblies; this was established by engineering a double-cysteine mutant in which the β-hairpin is stabilized by an intramolecular disulfide bond (48). Notably, the double-cysteine mutant $A\beta^{1-42}$ has been reported to form SDS-stable dimers/trimers, particularly trimers, which were absent in the mutant $A\beta^{1-40}$ (48). As a result, the mutant $A\beta^{1-42}$ forms highly neurotoxic, A11-negative, β-sheet-enriched assemblies of ~100 kDa (apparent mass on size exclusion chromatography) more readily than the mutant $A\beta^{1-40}$ does (48). Such conformational difference in $A\beta^{1-40}$ and $A\beta^{1-42}$ monomers might be reflected in the differences of ASPD formation. It is also possible that con-

formational differences in the initial monomer state might cause differences in dimer or trimer formation, leading to the distinct assembly pathways observed here. Further analysis, *e.g.* with NMR, is needed to elucidate the molecular mechanism of the differences.

To conclude, the observed differences in the assembly pathways clearly indicated that ASPDs are not fibril precursors, in accordance with the fact that ASPDs continued to exist after mature fibril formation without being incorporated into fibrils (5, 10). Our data also support the idea that the assembly pathway to ASPDs is different from the pathways leading to fibrils and to oligomers such as dimers and 12-mers (5, 10). As has also been suggested by others (45, 47, 48), our data further support the view that distinct assembly pathways lead to formation of assemblies with distinct tertiary structures (Fig. 4). We have thus discerned the different pathways by employing the combined FCS method, which should facilitate identifying the assembly steps where inhibition might be beneficial. This method should also be useful to find biological molecules or chemical factors that inhibit formation of these nonfibrillar Aβ assemblies and offers the potential for developing therapeutic agents based on this mechanistic understanding.

Acknowledgments—We thank A. Noguchi (Mitsubishi Kagaku Institute of Life Sciences) for technical help with IP; Dr. M. Noda (Mitsubishi Tanabe Pharma Corp.) for haASD1 antibody; Drs. Y. Kobayashi, H. Yokozawa, and K. Kanda (Mitsubishi Chemical Group Science and Technology Research Center) for technical help with atomic force microscopy and for computational set-up, respectively; and Drs. Y. Ishii (University of Illinois) and Y. Fujiyoshi (Kyoto University) for valuable discussions.

REFERENCES

1. Selkoe, D. J. (1991) *Neuron* **6,** 487–498
2. Ross, C. A., and Poirier, M. A. (2005) *Nat. Rev. Mol. Cell Biol.* **6,** 891–898
3. Lansbury, P. T., and Lashuel, H. A. (2006) *Nature* **443,** 774–779
4. Chiti, F., and Dobson, C. M. (2009) *Nat. Chem. Biol.* **5,** 15–22
5. Roychaudhuri, R., Yang, M., Hoshi, M. M., and Teplow, D. B. (2009) *J. Biol. Chem.* **284,** 4749–4753
6. Levine, H., 3rd (1995) *Neurobiol. Aging* **16,** 755–764
7. Podlisny, M. B., Ostaszewski, B. L., Squazzo, S. L., Koo, E. H., Rydell, R. E., Teplow, D. B., and Selkoe, D. J. (1995) *J. Biol. Chem.* **270,** 9564–9570
8. Walsh, D. M., Lomakin, A., Benedek, G. B., Condron, M. M., and Teplow, D. B. (1997) *J. Biol. Chem.* **272,** 22364–22372
9. Lambert, M. P., Barlow, A. K., Chromy, B. A., Edwards, C., Freed, R., Liosatos, M., Morgan, T. E., Rozovsky, I., Trommer, B., Viola, K. L., Wals, P., Zhang, C., Finch, C. E., Krafft, G. A., and Klein, W. L. (1998) *Proc. Natl. Acad. Sci. U.S.A.* **95,** 6448–6453
10. Hoshi, M., Sato, M., Matsumoto, S., Noguchi, A., Yasutake, K., Yoshida, N., and Sato, K. (2003) *Proc. Natl. Acad. Sci. U.S.A.* **100,** 6370–6375
11. Kayed, R., Head, E., Thompson, J. L., McIntire, T. M., Milton, S. C., Cotman, C. W., and Glabe, C. G. (2003) *Science* **300,** 486–489
12. Barghorn, S., Nimmrich, V., Striebinger, A., Krantz, C., Keller, P., Janson, B., Bahr, M., Schmidt, M., Bitner, R. S., Harlan, J., Barlow, E., Ebert, U., and Hillen, H. (2005) *J. Neurochem.* **95,** 834–847
13. Lesné, S., Koh, M. T., Kotilinek, L., Kayed, R., Glabe, C. G., Yang, A., Gallagher, M., and Ashe, K. H. (2006) *Nature* **440,** 352–357
14. Chimon, S., Shaibat, M. A., Jones, C. R., Calero, D. C., Aizezi, B., and Ishii, Y. (2007) *Nat. Struct. Mol. Biol.* **14,** 1157–1164
15. Deshpande, A., Mina, E., Glabe, C., and Busciglio, J. (2006) *J. Neurosci.* **26,** 6011–6018
16. Lacor, P. N., Buniel, M. C., Furlow, P. W., Clemente, A. S., Velasco, P. T., Wood, M., Viola, K. L., and Klein, W. L. (2007) *J. Neurosci.* **27,** 796–807
17. Shankar, G. M., Bloodgood, B. L., Townsend, M., Walsh, D. M., Selkoe, D. J., and Sabatini, B. L. (2007) *J. Neurosci.* **27,** 2866–2875
18. Shankar, G. M., Li, S., Mehta, T. H., Garcia-Munoz, A., Shepardson, N. E., Smith, I., Brett, F. M., Farrell, M. A., Rowan, M. J., Lemere, C. A., Regan, C. M., Walsh, D. M., Sabatini, B. L., and Selkoe, D. J. (2008) *Nat. Med.* **14,** 837–842
19. Perrin, R. J., Fagan, A. M., and Holtzman, D. M. (2009) *Nature* **461,** 916–922
20. Walsh, D. M., and Selkoe, D. J. (2007) *J. Neurochem.* **101,** 1172–1184
21. Noguchi, A., Matsumura, S., Dezawa, M., Tada, M., Yanazawa, M., Ito, A., Akioka, M., Kikuchi, S., Sato, M., Ideno, S., Noda, M., Fukunari, A., Muramatsu, S., Itokazu, Y., Sato, K., Takahashi, H., Teplow, D. B., Nabeshima, Y., Kakita, A., Imahori, K., and Hoshi, M. (2009) *J. Biol. Chem.* **284,** 32895–32905
22. Ashe, K. H. (2001) *Learn Mem.* **8,** 301–308
23. Hardy, J., and Selkoe, D. J. (2002) *Science* **297,** 353–356
24. Klein, W. L., Stine, W. B., Jr., and Teplow, D. B. (2004) *Neurobiol. Aging* **25,** 569–580
25. Glabe, C. G. (2006) *Neurobiol. Aging* **27,** 570–575
26. Gösch, M., and Rigler, R. (2005) *Adv. Drug Deliv. Rev.* **57,** 169–190
27. Björling, S., Kinjo, M., Földes-Papp, Z., Hagman, E., Thyberg, P., and Rigler, R. (1998) *Biochemistry* **37,** 12971–12978
28. Bark, N., Földes-Papp, Z., and Rigler, R. (1999) *Biochem. Biophys. Res. Commun.* **260,** 35–41
29. Tjernberg, L. O., Pramanik, A., Björling, S., Thyberg, P., Thyberg, J., Nordstedt, C., Berndt, K. D., Terenius, L., and Rigler, R. (1999) *Chem. Biol.* **6,** 53–62
30. Pitschke, M., Prior, R., Haupt, M., and Riesner, D. (1998) *Nat. Med.* **4,** 832–834
31. Sengupta, P., Garai, K., Sahoo, B., Shi, Y., Callaway, D. J., and Maiti, S. (2003) *Biochemistry* **42,** 10506–10513
32. Provencher, S. W. (1982) *Comput. Phys. Commun.* **27,** 213–227
33. Provencher, S. W. (1982) *Comput. Phys. Commun.* **27,** 229–242
34. Palmer, A. G., 3rd, and Thompson, N. L. (1987) *Biophys. J.* **52,** 257–270
35. Walsh, D. M., Hartley, D. M., Kusumoto, Y., Fezoui, Y., Condron, M. M., Lomakin, A., Benedek, G. B., Selkoe, D. J., and Teplow, D. B. (1999) *J. Biol. Chem.* **274,** 25945–25952
36. Lomakin, A., Chung, D. S., Benedek, G. B., Kirschner, D. A., and Teplow, D. B. (1996) *Proc. Natl. Acad. Sci. U.S.A.* **93,** 1125–1129
37. LeVine, H., 3rd (1993) *Protein Sci.* **2,** 404–410
38. Tjernberg, L. O., Näslund, J., Lindqvist, F., Johansson, J., Karlström, A. R., Thyberg, J., Terenius, L., and Nordstedt, C. (1996) *J. Biol. Chem.* **271,** 8545–8548
39. Klein, W. L., Krafft, G. A., and Finch, C. E. (2001) *Trends Neurosci.* **24,** 219–224
40. Glabe, C. G. (2008) *J. Biol. Chem.* **283,** 29639–29643
41. Hepler, R. W., Grimm, K. M., Nahas, D. D., Breese, R., Dodson, E. C., Acton, P., Keller, P. M., Yeager, M., Wang, H., Shughrue, P., Kinney, G., and Joyce, J. G. (2006) *Biochemistry* **45,** 15157–15167
42. Bitan, G., Vollers, S. S., and Teplow, D. B. (2003) *J. Biol. Chem.* **278,** 34882–34889
43. Grant, M. A., Lazo, N. D., Lomakin, A., Condron, M. M., Arai, H., Yamin, G., Rigby, A. C., and Teplow, D. B. (2007) *Proc. Natl. Acad. Sci. U.S.A.* **104,** 16522–16527
44. Ono, K., Condron, M. M., and Teplow, D. B. (2009) *Proc. Natl. Acad. Sci. U.S.A.* **106,** 14745–14750
45. Bernstein, S. L., Dupuis, N. F., Lazo, N. D., Wyttenbach, T., Condron, M. M., Bitan, G., Teplow, D. B., Shea, J. E., Ruotolo, B. T., Robinson, C. V., and Bowers, M. T. (2009) *Nat. Chem.* **1,** 326–331
46. O'Nuallain, B., Freir, D. B., Nicoll, A. J., Risse, E., Ferguson, N., Herron, C. E., Collinge, J., and Walsh, D. M. (2010) *J. Neurosci.* **30,** 14411–14419
47. Chen, Y. R., and Glabe, C. G. (2006) *J. Biol. Chem.* **281,** 24414–24422
48. Sandberg, A., Luheshi, L. M., Söllvander, S., Pereira de Barros, T., Macao, B., Knowles, T. P., Biverstål, H., Lendel, C., Ekholm-Petterson, F., Dubnovitsky, A., Lannfelt, L., Dobson, C. M., and Härd, T. (2010) *Proc. Natl. Acad. Sci. U.S.A.* **107,** 15595–15600

DOI: 10.1002/cbic.200900649

Application of a Stimuli-Responsive Polymer to the Development of Novel MRI Probes

Satoshi Okada, Shin Mizukami, and Kazuya Kikuchi*[a]

Magnetic resonance imaging is a medical diagnostic tool that is attracting considerable attention as a molecular-imaging technique; this is because MRI is a noninvasive imaging technique that provides information about the internal structure of living organisms. Recently, various chemically modified MRI contrast agents have been developed in order to study in vivo phenomena. These contrast agents, termed "MRI probes", have various functions and include probes that detect enzyme activities, variations in pH, the ionic concentration, and so on.[1] In order to change the probes' relaxivities by external stimuli, probes were designed to accommodate a certain number of bound water molecules per gadolinium ion.[1a] Other probes involved the attachment of macromolecules, such as proteins, to change the molecular mobility of the probe.[1i] However, the rational development of such MRI probes is at an early stage, and the strategies for developing MRI probes are limited.

In order to design novel MRI probes, we focused our attention on stimuli-responsive polymers, which can change their conformation in response to external stimuli such as chemicals, temperature, and pH.[2] Stimuli-responsive polymers that exhibit large conformational changes have been developed for applications in drug-delivery systems, functional polymeric matrices, and artificial tissues. To the best of our knowledge, there has been no report regarding the application of stimuli-responsive polymers to the development of MRI probes. In this study, a novel MRI probe was developed by employing a strategy based on conformational changes in stimuli-responsive polymers. We demonstrated that this principle of probe design is useful in detecting pH changes. Additionally, we investigated in detail the stimuli-responsive mechanism of the probe.

pH-responsive polymers were chosen for the development of the probe due to their high potential in clinical applicability for monitoring diseases such as kidney disorder and cancer. The relaxivities of MRI probes are influenced by their rotational motions; therefore, if a pH-responsive conformational change in the probe induces rotational mobility of the Gd^{III} complexes attached to the probe, pH variations would lead to alterations in the probe relaxivity. We designed a pH-responsive MRI probe, P-Gd, by attaching clinically used Gd^{III} complexes and dansyl chromophores to a pH-responsive polymer, *n*-octylamine-modified poly(sodium maleate-*alt*-ethyl vinyl ether) (poly(SM-EVE); Figure 1). At a low pH, *n*-octylamine-modified poly(SM-EVE) takes on a compact globule conformation because of the intramolecular hydrophobic interactions among the *n*-octyl groups.[3] In contrast, at a high pH, the polymer conformation expands because of the electrostatic repulsion among the deprotonated carboxy groups. Therefore, it is assumed that the molecular rotation of the side chains of the polymer is restricted at low pH, and that the side chains in the expanded conformation rotate more rapidly at a high pH.

In order to elucidate the pH-dependent changes in the polymer shape, we synthesized an aminoethyl-modified Gd(DO3A) complex (Gd(AEDO3A)) and dansyl ethylenediamine, as previously described by Li et al.[4] and Shea et al.,[5] respectively. Platform polymer poly(SM-EVE) anhydride was synthesized and then modified with *n*-octylamine according to the scheme reported by Hu et al.[6] After attaching the Gd^{III} complexes and the dansyl chromophores to the *n*-octylamine-modified polymers, the residual carboxylic anhydride groups in the polymer were hydrolyzed with 1 M aqueous NaOH. The polymers were dialyzed and lyophilized to yield P-Gd (Scheme S1 in the Supporting Information). Constituents of octyl groups and Gd^{III} were estimated by using elemental analysis and ICP-MS. The approximate molecular weight of the platform polymer was determined by GPC after it was hydrolyzed by the alkaline aqueous solution.

Thereafter, in order to demonstrate the possibility of using P-Gd as a pH-responsive MRI probe, the relaxivities of P-Gd at pH 4–10 were measured. The longditudinal and transverse relaxivities (r_1 and r_2, respectively) increased as the pH decreased and were maximal at pH 4, while the relaxivities of Gd(AEDO3A) did not increase (Figure 2). This result is consistent with the expected pH-responsive behavior of *n*-octylamine-modified poly(SM-EVE).[3] It is assumed that the limited rotational motion of the side chains caused the increase in relaxivities at a low pH. By replacing the carboxy groups of the polymer side chains with functional groups whose pK_a is near to physiological pH, such as sulfonamide, P-Gd could allow pathological tissues in which the extracellular pH is acidic to be imaged.

The mechanism of variation in relaxation time was investigated as follows. In order to verify the conformational change in P-Gd, its fluorescence spectra were measured. The dansyl group is known to be an environmentally sensitive chromophore. The fluorescence emission spectra of the dansyl group exhibit a blue shift and their intensity increases as the group's surroundings become hydrophobic.[7] Therefore, we can obtain information about the conformation of P-Gd from the emission spectra of the dansyl groups attached to the polymer side chains. As the solution pH decreased, the emission spectra of P-Gd exhibited a shift toward shorter wavelengths with an increase in the fluorescence intensity, while the emission spectra of *N*-acetyl-*N'*-dansyl ethylenediamine, which is a monomer

[a] *S. Okada, Dr. S. Mizukami, Prof. K. Kikuchi*
Graduate School of Engineering, Osaka University
2-1 Yamadaoka, Suita City, Osaka 565-0871 (Japan)
Fax: (+81) 6-6879-7875
E-mail: kkikuchi@mls.eng.osaka-u.ac.jp

Supporting information for this article is available on the WWW under http://dx.doi.org/10.1002/cbic.200900775.

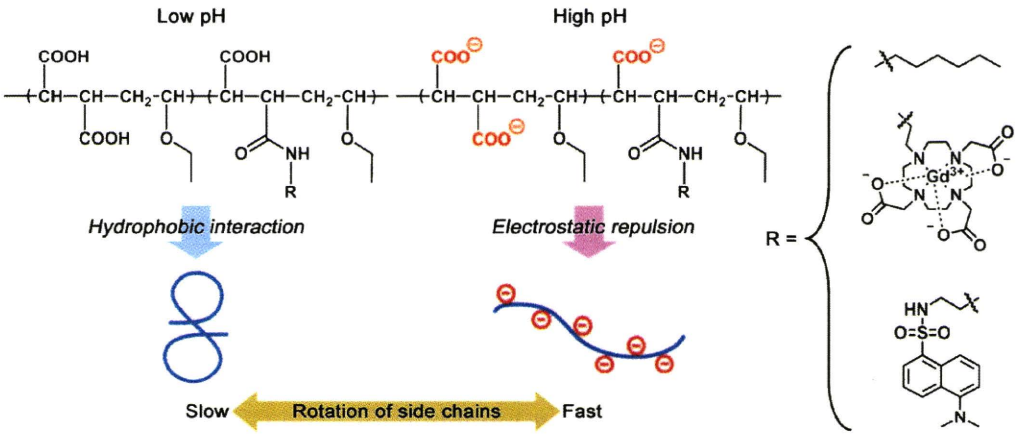

Figure 1. pH-responsive conformational change in the *n*-octylamine-modified poly(SM-EVE)-based MRI probe, P-Gd.

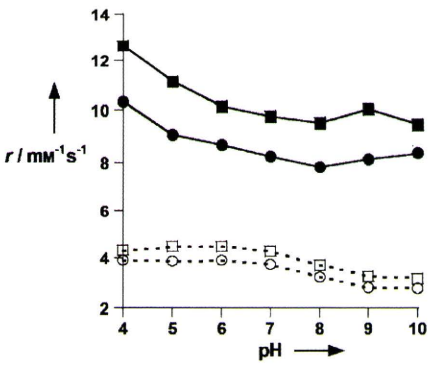

Figure 2. pH profile of the relaxivities of P-Gd (filled symbols) and Gd-(AEDO3A) (open symbols) at 20 MHz and 37 °C. *r* is expressed per Gd^{III} ion; circles: r_1, squares: r_2.

model compound of P-Gd, did not shift or increase (Figure 3). These results indicate the build up of a hydrophobic environment around the dansyl groups as the P-Gd conformation becomes globular at a low pH. In contrast, P-Gd expanded in alkaline solution, and the emission spectra indicate the presence of a hydrophilic environment around the dansyl groups. This conformational change is the result of the intramolecular electrostatic repulsion of the carboxylate anions.

In order to reveal the correlation between the probe relaxivity and the polymer mobility, we estimated the rotational correlation times, τ_R, of the polymer side chains at different pHs. τ_R, which indicates the mobility of the polymer side chains, can be estimated from the values of the fluorescence anisotropy *r* and the fluorescence lifetime τ_F of P-Gd by using the Perrin–Weber equation [Eq. (1)].[8]

$$r_0/r = 1 + \tau_F/\tau_R \quad (1)$$

Here, r_0 represents the limiting value of *r* in a medium where no rotational diffusion occurs and where the Brownian motion is frozen. r_0 for the dansyl chromophore was experimentally determined to be 0.325.[9] After the fluorescence anisotropy and fluorescence lifetime values had been determined (Figures S1 and S3), the rotational correlation times were calculated and plotted against different pH values (Figure 4). The rotational correlation times varied on a nanosecond timescale

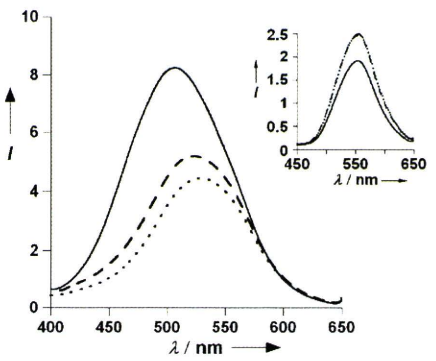

Figure 3. Fluorescence spectra of 0.05% (*w/v*) P-Gd and 25 μM *N*-acetyl-*N'*-dansyl ethylenediamine in 100 mM phosphate buffer at 37 °C. $\lambda_{ex} = 330$ nm; ——: pH 4, - - - - -: pH 6, ····: pH 8. Inset: *N*-acetyl-*N'*-dansyl ethylenediamine.

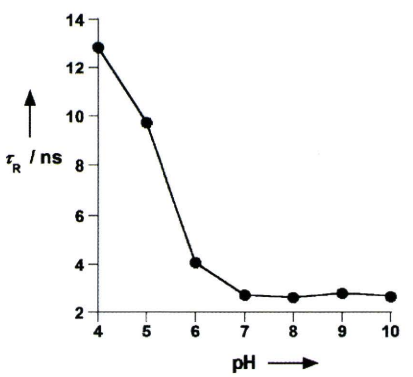

Figure 4. Rotational correlation times of P-Gd in 100 mM phosphate buffer at 25 °C.

and increased at low pH. The pH profile of the rotational correlation time agrees closely with the pH profile of the relaxivity (Figure 2). The rotational correlation times of standard small-molecule contrast agents such as Gd(DOTA)$^-$ are on the picosecond timescale.[10] Because the rotational correlation time of P-Gd is higher than that of the small-molecule contrast agent, the relaxivity of the former is higher than that of the latter.

In conclusion, a novel stimuli-responsive MRI probe has been developed by using a pH-responsive polymer. The relaxivity of the probe was observed to increase with a decrease in the pH of the solution. This pH-responsive mechanism was evaluated in detail through fluorescence studies, which demonstrated that the pH-responsive conformational change caused a change in the rotational correlation time. Thus, we can conclude that relaxivity is pH-dependent. This novel principle of stimuli-responsive polymer conformational change could become a new design strategy for MRI probes or lead to the development of new functional MRI probes.

Experimental Section

Fluorescence anisotropy r was measured at pH 4–10 and 25 °C. The fluorescence anisotropy increased as the pH decreased from 7 (Figure S1), thus indicating that, while the rotational motion of the side chains is more pronounced at a high pH, it is restricted at a low pH.

The fluorescence decay curves of P-Gd were acquired in phosphate buffer (100 mM, pH 4–10) at 25 °C (shown in Figure S2 and fitted with double-exponential components; Equation (2)). One of the two components τ_1 has a long fluorescence lifetime value of ~25 ns, while the other τ_2 has a short fluorescence lifetime value of ~7 ns. The long-lifetime component increased, its ratio expressed by $A_1/(A_1+A_2)$, as the pH decreased. Therefore, the long-lifetime component is consistent with the dansyl groups existing in a hydrophobic environment. In contrast, the short-lifetime component indicates that the dansyl groups were exposed to the aqueous environment.

$$I(t) = A_1 \exp(-t/\tau_1) + A_2 \exp(-t/\tau_2) \quad (2)$$

The weighted-average lifetime was calculated from Equation (3). The fluorescence lifetime grew longer with a decrease in the pH value (Figure S3). This indicates that the environment around the dansyl groups changed due to the conformational change of P-Gd.

$$\tau_F = \tau_1 A_1/(A_1 + A_2) + \tau_2 A_2/(A_1 + A_2) \quad (3)$$

Acknowledgements

We thank Dr. Kei Ohkubo and Prof. Shunichi Fukuzumi at Osaka University for fluorescence lifetime measurements. S.O. expresses his special thanks for the Global COE Program "Global Education and Research Center for Bio-Environmental Chemistry" of Osaka University.

Keywords: contrast agents · MRI · polymers · relaxivity · rotational correlation time

[1] a) A. Y. Louie, M. M. Hüber, E. T. Ahrens, U. Rothbächer, R. Moats, R. E. Jacobs, S. E. Fraser, T. J. Meade, *Nat. Biotechnol.* **2000**, *18*, 321; b) J. M. Perez, L. Josephson, T. O'Loughlin, D. Högemann, R. Weissleder, *Nat. Biotechnol.* **2002**, *20*, 816; c) W.-h. Li, S. E. Fraser, T. J. Meade, *J. Am. Chem. Soc.* **1999**, *121*, 1413; d) S. Zhang, K. Wu, A. D. Sherry, *Angew. Chem.* **1999**, *111*, 3382; *Angew. Chem. Int. Ed.* **1999**, *38*, 3192; e) S. Aime, A. Barge, D. D. Castelli, F. Fedeli, A. Mortillaro, F. U. Nielsen, E. Terreno, *Magn. Reson. Med.* **2002**, *47*, 639; f) P. Caravan, B. Das, S. Dumas, F. H. Epstein, P. A. Helm, V. Jacques, S. Koerner, A. Kolodziej, L. Shen, W.-C. Sun, Z. Zhang, *Angew. Chem.* **2007**, *119*, 8319; *Angew. Chem. Int. Ed.* **2007**, *46*, 8171; g) G. Liu, Y. Li, M. D. Pagel, *Magn. Reson. Med.* **2007**, *58*, 1249; h) T. Chauvin, P. Durand, M. Bernier, H. Meudal, B.-T. Doan, F. Noury, B. Badet, J.-C. Beloeil, É. Tóth, *Angew. Chem.* **2008**, *120*, 4442; *Angew. Chem. Int. Ed.* **2008**, *47*, 4370; i) K. Hanaoka, K. Kikuchi, T. Terai, T. Komatsu, T. Nagano, *Chem. Eur. J.* **2008**, *14*, 987.

[2] a) S. Han, M. Hagiwara, T. Ishizone, *Macromolecules* **2003**, *36*, 8312; b) D. Neradovic, C. F. v. Nostrum, W. E. Hennink, *Macromolecules* **2001**, *34*, 7589; c) S. Y. Park, Y. H. Bae, *Macromol. Rapid Commun.* **1999**, *20*, 269; d) L.-C. You, F.-Z. Lu, Z.-C. Li, W. Zhang, F.-M. Li, *Macromolecules* **2003**, *36*, 1; e) T. Miyata, N. Asami, T. Uragami, *Nature* **1999**, *399*, 766.

[3] Y. Hu, R. S. Armentrout, C. L. McCormick, *Macromolecules* **1997**, *30*, 3538.

[4] C. Li, Y.-X. Li, G.-L. Law, K. Man, W.-T. Wong, H. Lei, *Bioconjugate Chem.* **2006**, *17*, 571.

[5] K. J. Shea, G. J. Stoddard, D. M. Shavelle, F. Wakui, R. M. Choate, *Macromolecules* **1990**, *23*, 4497.

[6] Y. Hu, M. C. Kramer, C. J. Boudreaux, C. L. McCormick, *Macromolecules* **1995**, *28*, 7100.

[7] Y.-H. Li, L.-M. Chan, L. Tyer, R. T. Moody, C. M. Himel, D. M. Hercules, *J. Am. Chem. Soc.* **1975**, *97*, 3118.

[8] G. Weber, *Biochem. J.* **1952**, *51*, 145.

[9] Y. Hu, K. Horie, H. Ushiki, *Macromolecules* **1992**, *25*, 6040.

[10] C. F. G. C. Geraldes, A. D. Sherry, I. Lázár, A. Miseta, P. Bogner, E. Berenyi, B. Sumegi, G. E. Kiefer, K. McMillan, F. Maton, R. N. Muller, *Magn. Reson. Med.* **1993**, *30*, 696.

Received: October 23, 2009
Revised: February 23, 2010
Published online on March 5, 2010

Multicolor Protein Labeling in Living Cells Using Mutant β-Lactamase-Tag Technology

Shuji Watanabe,[†] Shin Mizukami,[†,‡] Yuichiro Hori,[†] and Kazuya Kikuchi*[,†,‡]

Division of Advanced Science and Biotechnology, Graduate School of Engineering, and Immunology Frontier Research Center, Osaka University, 2-1 Yamadaoka, Suita, Osaka, 565-0871, Japan. Received July 29, 2010; Revised Manuscript Received September 21, 2010

Protein labeling techniques using small molecule probes have become important as practical alternatives to the use of fluorescent proteins (FPs) in live cell imaging. These labeling techniques can be applied to more sophisticated fluorescence imaging studies such as pulse-chase imaging. Previously, we reported a novel protein labeling system based on the combination of a mutant β-lactamase (BL-tag) with coumarin-derivatized probes and its application to specific protein labeling on cell membranes. In this paper, we demonstrated the broad applicability of our BL-tag technology to live cell imaging by the development of a series of fluorescence labeling probes for this technology, and the examination of the functions of target proteins. These new probes have a fluorescein or rhodamine chromophore, each of which provides enhanced photophysical properties relative to coumarins for the purpose of cellular imaging. These probes were used to specifically label the BL-tag protein and could be used with other small molecule fluorescent probes. Simultaneous labeling using our new probes with another protein labeling technology was found to be effective. In addition, it was also confirmed that this technology has a low interference with respect to the functions of target proteins in comparison to GFP. Highly specific and fast covalent labeling properties of this labeling technology is expected to provide robust tools for investigating protein functions in living cells, and future applications can be improved by combining the BL-tag technology with conventional imaging techniques. The combination of probe synthesis and molecular biology techniques provides the advantages of both techniques and can enable the design of experiments that cannot currently be performed using existing tools.

INTRODUCTION

Recent prominent advances in fluorescence imaging techniques enabled investigations of direct localization and trafficking of biomolecules in living cells. Genetic engineering has also been progressing dramatically and provides methods for expressing various proteins in specific organelles in cells. Fusion proteins prepared by linkage of fluorescent proteins (FPs) can be used to obtain tools for imaging any protein of interest (POI) (*1*). However, it is difficult to use FPs in pulse-chase imaging studies for investigating protein function over time within the space inside a living cell and to optimize fluorescence properties such as emission and excitation wavelengths, extinction coefficients, and photostability for various experiments. Moreover, certain FPs tend to form protein aggregates that affect the function and/or localization of the target POIs (*2, 3*).

Protein labeling methods using small molecule probes have attracted great attention because they may have the ability to overcome the limitations of FPs. Several methods for labeling proteins with small molecules have been commercialized, including Lumio-tag (*4*−*6*), HaloTag (*7*), SNAP-tag (*8*−*10*), and DHFR-based tag (*11*). Lumio-tag, using FlAsH or ReAsH, is based upon a fluorescent biarsenical dye that reacts with tetracysteine peptide and generates strong fluorescence. HaloTag is a modified haloalkane dehalogenase designed to covalently react with synthetic haloalkyl ligands. SNAP-tag utilizes human O^6-alkylguanine-DNA-alkyltransferase (hAGT) as the protein tagged with synthetic benzylguanine derivatives. DHFR-based tag employs the noncovalent interaction between *Escherichia coli* dihydrofolate reductase and fluorescently labeled methotrexate. Other protein labeling methods based on biotin ligase (*12*), transglutaminase (*13*), hexahistidine (*14*), and tetraaspartic acid (*15*) have also been reported.

The advantages of synthetic fluorescent probes are tunable switches for changes in fluorescence characteristics. These probes have intense fluorescence properties and provide a wide range of choices in fluorophores. Meanwhile, the advantages of using protein expression systems are provided by specific expression in cellular components and tissues, convenient experimental procedures, and the potential for in vivo studies using transgenic mice. Combining the advantages of both techniques is expected to provide enhanced methods for exploring molecular functions in biological systems.

For incorporation of the tunable switches in expressed protein tags, we previously reported a specific protein labeling system with an off/on fluorescence switch that employs a mutant enzyme and its specific substrate. The system involves covalent modification of a mutant β-lactamase (BL-tag) with a rationally designed fluorogenic probe based on fluorescence resonance energy transfer (FRET) (*16*). β-Lactamases are members of a family of bacterial enzymes that efficiently cleave β-lactam moieties within compounds such as penicillins and cephalosporins (*17*). Since the activity of β-lactamases is not observed in eukaryotic cells, these proteins have been widely exploited as reporter enzymes in living mammalian cells (*18*−*20*). Furthermore, their three-dimensional structures, catalytic mechanism, and inhibitors have been widely studied because of their clinical importance (*21*). A well-characterized isoform is the 29 kDa TEM-1 β-lactamase from *Escherichia coli* categorized as a class A β-lactamase (*22*).

* E-mail: kkikuchi@mls.eng.osaka-u.ac.jp. Phone: +81-6-6879-7924. Fax: +81-6-6879-7875.

[†] Division of Advanced Science and Biotechnology.

[‡] Immunology Frontier Research Center.

10.1021/bc100333k
Published on Web 10/20/2010

Scheme 1. Reaction Mechanism of Wild-Type (WT) and Mutant (E166N) TEM-1 β-Lactamase

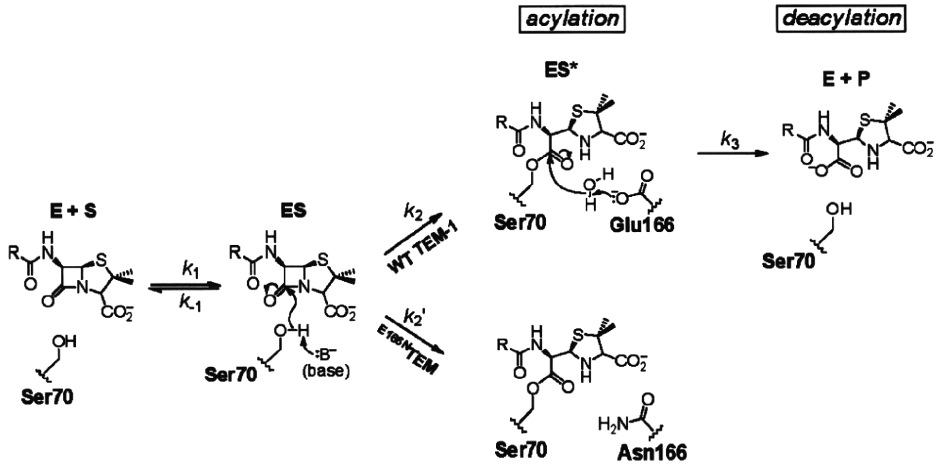

The reaction of wild-type (WT) TEM-1 with β-lactams involves acylation and deacylation steps (Scheme 1). Nucleophilic attack on the β-lactam ring by Ser70 leads to the covalent acyl-enzyme intermediate. In WT TEM-1, Glu166 acts as a base to catalyze hydrolysis of the intermediate (*23*), resulting in release of the product and regeneration of WT TEM-1. In ^{E166N}TEM, Asn166 is ineffective as a base; hence, the intermediate accumulates as a stable covalent adduct (*24*).

According to the above-mentioned mechanism, we have reported a novel protein labeling system with an off−on fluorescence switch based on a combination of a mutant β-lactamase (BL-tag) and coumarin-based substrates. Owing to the rational design of both the tag protein and the labeling probes, this system enabled us to simultaneously achieve specific and fluorogenic labeling of the target protein on living cells (*16*). In our previous report, we designed and synthesized both a simple fluorescent labeling probe, designated CA, and a fluorogenic probe, designated CCD. CA is a 7-hydroxycoumarin−ampicillin conjugate and CCD includes three main components; 7-hydroxycoumarin, cephalosporin, and DABCYL. The fluorescence of CCD is largely quenched by intramolecular FRET from coumarin to DABCYL. Cleavage of the cephalosporin β-lactam ring produces a free amino group, which triggers spontaneous elimination of any leaving group previously attached to the 3′ position (*25*). Consequently, fluorogenic labeling with CCD of fusion proteins of ^{E166N}TEM (BL-tag) was successfully performed in vitro and on the surfaces of living cells.

In this paper, we demonstrated the broad applicability of this labeling technology for live cell imaging experiments by developing a series of labeling probes with various fluorophores. We also show that this technology has a low interference with respect to the functions of EGFR and is orthogonal to another currently used protein labeling method.

EXPERIMENTAL PROCEDURES

Fluorometric Analysis. The slit width was 2.5 nm for both excitation and emission, and the photomultiplier voltage was 700 V. All fluorescent probes were dissolved in DMSO to obtain 10 mM stock solutions, and these solutions were diluted to the desired final concentrations with an appropriate aqueous buffer solution. Relative fluorescence quantum yields of the compounds were obtained by comparing the area under the emission spectrum of the sample with that of an EtOH solution of rhodamine B, which has a quantum efficiency of 0.97 when excited at 545 nm (*26*), and with that of a 100 mM NaOH solution of fluorescein, which has a quantum efficiency of 0.85 when excited at 492 nm (*27*).

Calculation of Förster Distance (R_0) and Energy Transfer Efficiency (E). For evaluation of R_0 and E, a revised version of the Förster formula was used (*28*)

$$R_0 = 9.78 \times 10^3(\Phi_D\kappa^2 n^{-4} J)^{1/6} \quad \left(J = \int_0^\infty f_D(\lambda)\varepsilon_A\lambda^4\,d\lambda\right)$$

$$E = R_0^6/(R_0^6 + R^6)$$

where R_0 is expressed in Å units, κ^2 is the orientation factor, Φ_D is the donor quantum yield in the absence of acceptor, n is the refractive index of the medium, $f_D(\lambda)$ is the normalized donor emission spectrum, $\varepsilon_A(\lambda)$ is the acceptor molar absorption coefficient in M^{-1} cm^{-1} units, and R is the donor−acceptor distance. The wavelength is expressed in nanometer units. The value $\kappa^2 = 2/3$, which corresponds to a dynamic isotropic regime, was assumed and $n = 1.33$ was applied. The molar absorption coefficient (ε) of DABCYL was 25 500 (λ = 462 nm) in 100 mM HEPES buffer (pH 7.4). R_0 values were calculated for the CA-DABCYL pair for CCD, the FA-DABCYL pair for FCD, and the RA-DABCYL pair for RCD. The quantum yields (Φ_D) of the compounds were 0.40 for CA, 0.71 for FA, and 0.49 for RA. The donor−acceptor distance (R) was evaluated by using the integrated molecular modeling packages *Maestro* v 8.5 and *MacroModel* v 9.6.

HPLC Analysis. HPLC analyses were performed with an Inertsil ODS-3 (4.6 × 250 mm) column (GL Sciences Inc.) using an HPLC system that comprises a pump (PU-2080, JASCO) and a detector (MD-2010 or FP-2020, JASCO). Preparative HPLC was performed with an Inertsil ODS-3 (10.0 × 250 mm) column (GL Sciences Inc.) using an HPLC system that comprises a pump (PU-2087, JASCO) and a detector (UV-2075, JASCO).

Fluorescence Microscopy. Fluorescence microscopic images were recorded using a IX71 fluorescence microscope (Olympus), a Cool Snap HQ cooled CCD camera (Roper Scientific), and a USH-103OL mercury lamp (Olympus). The filter sets used were Olympus BP330-385, DM455, and BA455 for Hoechst 33342 and coumarin derivatives; BP470-495, DM505, and BA510-550 for fluorescein derivatives; and BP510-550, DM575, and BA575-625 for rhodamine derivatives. *MetaMorph* imaging software (Universal Imaging Corporation) was used for imaging and data analysis.

Detection of Protein Labeling by SDS-PAGE. WT TEM-1 or ^{E166N}TEM (*16*) (20 μM) was added to a solution of probes (30 μM) in 100 mM HEPES buffer (pH 7.4) at 25 °C. After 30 min, the labeled protein was denatured in 2 × SDS gel loading buffer (100 mM Tris−HCl buffer (pH 6.8), 2.5% SDS, 20%